BIOMATERIALS

Biohybrid hand actuated by multiple human muscle tissues

Xinzhu Ren[1], Yuya Morimoto[1,2], Shoji Takeuchi[1]*

Cultured muscle tissue serves as a power source in biohybrid robots that demonstrate diverse motions. However, current designs typically only drive simple substrates on a small scale, limiting flexibility and controllability. To address this, we proposed a biohybrid hand with multijointed fingers powered by multiple muscle tissue actuators (MuMuTAs), bundles of thin muscle tissues. The MuMuTA can provide linear actuation with high contractile force (~8 millinewtons) and high contractile length (~4 millimeters), which can be converted into the flexion of multijointed fingers by a cable-driven mechanism. We successfully powered the biohybrid hand achieving individual control of fingers and a variety of motions using different signaling controls. This study showcases the potential of MuMuTAs as a driving source for advanced biohybrid robotics.

INTRODUCTION

Skeletal muscles act as natural actuators to enable the fine and flexible actions of animal bodies (*1*). To mimic muscle-driven movements, biohybrid robots composed of muscles and artificial materials have been developed. Advances in bioengineering technology allow the creation of cultured muscle tissue (*2*–*6*) with a longer life span than that of excised muscle (*7*) because cultured tissue can obtain nutrients from the culture medium. This cultured muscle tissue can be used as a power source in a biohybrid robot incorporating a rigid skeleton with joints (*8*), a flexible rubber substrate (*9*–*16*), a paper substrate (*17*), and a combination of rigid skeletons and soft parts (*18*–*21*). Muscle contractions enable biohybrid robots to perform motions, such as moving in a dish (*11*, *12*), swimming (*9*, *17*), bipedal walking (*18*), manipulating objects (*8*, *10*, *19*), and multi–degree-of-freedom actuation (*20*). However, previous biohybrid robots have generally been only a few centimeters in size and featured simple structures with a single joint or hinge (*22*), making it impossible to move larger structures. Moving larger structures, such as a human hand with multiple joints, requires muscle tissue actuators with greater force and displacement capabilities. High contractile length can be achieved using longer muscle tissue because contractile length is dependent on muscle length (*23*). Although conventional studies have shown that muscle contractile force is proportional to the cross-sectional area (*24*), excessively thick muscle tissue suffers from necrosis because of insufficient nutrient and oxygen delivery (*25*). In addition, thinner muscle tissues have better muscle fiber orientation (*26*), improving contractile performance. Therefore, the accumulation of multiple thin and long muscle tissues can provide biohybrid actuators with high contractile force and high contractile length.

In this study, inspired by the living muscle structure, an aggregate of muscle fascicles that are bundles of myofibers (*27*), we proposed bundling several thin strands of muscle tissues to form a multiple muscle tissue actuator (MuMuTA). The MuMuTA contraction generates high contractile force, and the high orientation of myotubes in thin muscle tissues increases overall contractile length. These features make MuMuTAs a suitable power source for a larger-scale (>10 cm) artificial robot hand. Using a cable-driven mechanism, the linear actuation of a MuMuTA can be converted into the rotation of multiple joints in the fingers, thus achieving a biohybrid hand driven by muscle contractions. It is important to note that previous biohybrid robots have generally been around a few centimeters in size, making it impossible to move larger structures. The high output performance of the MuMuTA allowed us to create larger biohybrid robots. Here, we developed an 18-cm biohybrid hand powered by MuMuTAs and demonstrated that the biohybrid hand can selectively move each finger and manipulate objects.

RESULTS

Construction of a biohybrid hand powered by MuMuTAs

The biohybrid hand with five biohybrid fingers operated in the culture medium (Fig. 1A and fig. S1). Each biohybrid finger had a multijointed finger skeleton and a MuMuTA connected by a tendon-like structure. MuMuTAs were mounted on the forearm part of a hand substrate, with a pair of gold electrodes diagonally inserted on both sides of each MuMuTA. Glass slides placed outside the electrodes acted as walls to limit the electric field's diffusion. The MuMuTA comprised multiple thin human skeletal muscle tissues and a pair of anchor holders (Fig. 1B). The anchor holder was formed by connecting 3D-printed parts with a flexible ribbon (fig. S2), and the anchors at the ends of muscle tissues were immobilized on the pair of anchor holders to form a multiple muscle tissue sheet (MuMuSheet). Therefore, by rolling up the MuMuSheet like a sushi roll and inserting two rods to maintain the shape, we succeeded in the construction of the MuMuTA (Fig. 1C).

One end of the MuMuTA was fixed, and a float was attached to the other end, keeping the contraction direction parallel to the liquid surface. When electrically stimulated, the MuMuTA contracted, pulling the tendon-like structure attached to the fingertip and bending the finger (Fig. 1D). Despite slight variations in size, each biohybrid finger shared the above configuration and driving principle, mimicking a simplified human tendon-driven structure (*28*). As a result of mounting five biohybrid fingers on the hand substrate, the preparation of the biohybrid hand was achieved (Fig. 1E).

Characteristics of human skeletal muscle tissue

We constructed muscle tissues in polydimethylsiloxane (PDMS) molds and cultured them on a flat culture platform called the MuMuTA

[1]Department of Mechano-Informatics, Graduate School of Information Science and Technology, University of Tokyo, Tokyo, Japan. [2]Department of Electronic and Physical Systems, School of Fundamental Science and Engineering, Waseda University, Tokyo, Japan.
*Corresponding author. Email: takeuchi@hybrid.t.u-tokyo.ac.jp

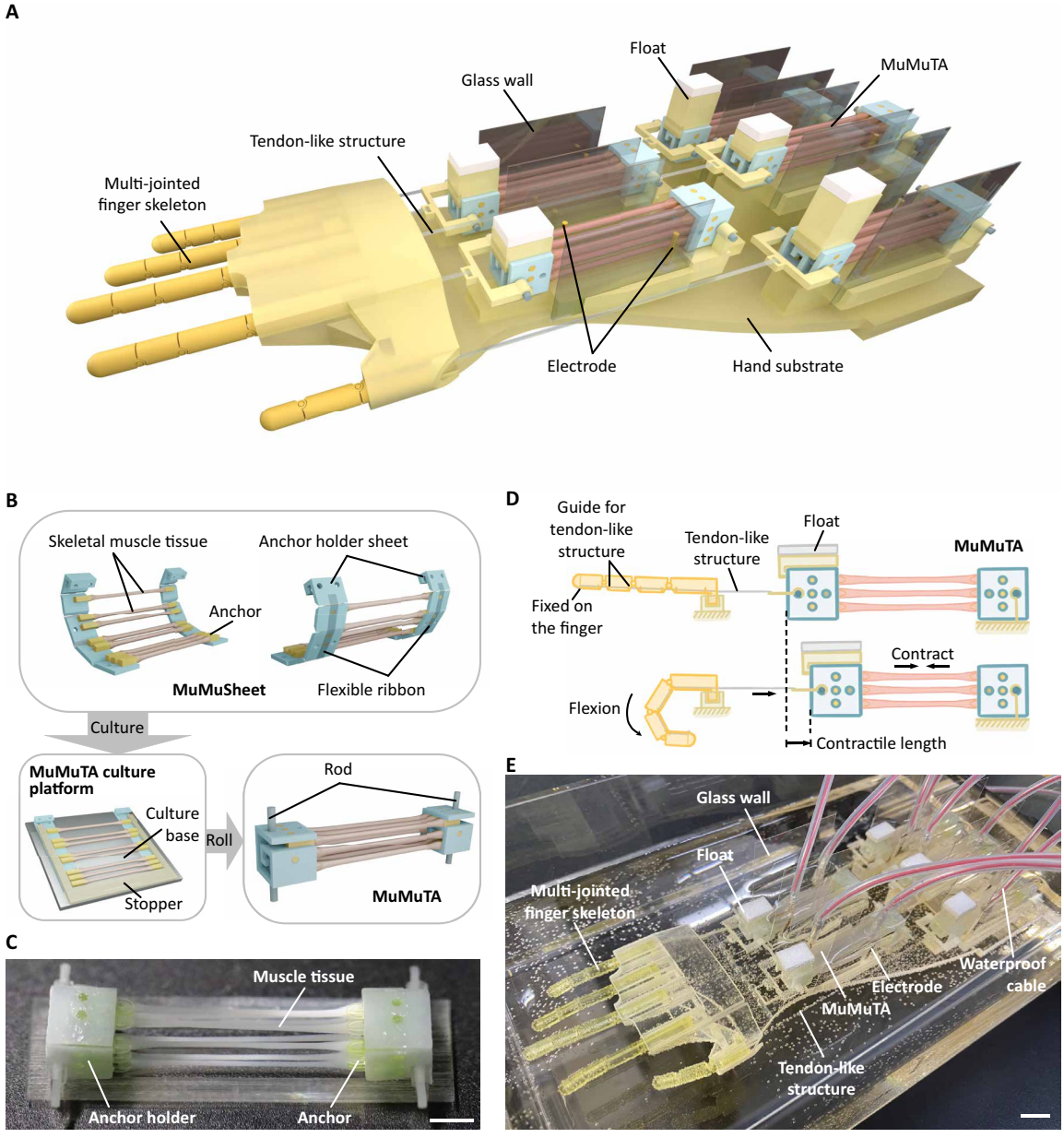

Fig. 1. Construction of a biohybrid hand powered by MuMuTAs. (**A**) Conceptual illustration of the biohybrid hand. (**B**) Construction of a MuMuTA composed of a pair of anchor holders arranged in parallel with eight muscle tissues from a MuMuSheet. Rolling the MuMuSheet up formed a MuMuTA. (**C**) Image of a MuMuTA. Rolled anchor holders are fixed. Eight muscle tissues stay parallel with each other between the anchor holders. Scale bar, 5 mm. (**D**) Conceptual diagram of the MuMuTA driving finger bending through a cable-driven mechanism. (**E**) Image of the biohybrid hand. Each electrode links to a waterproof cable to receive electrical stimulation. Scale bar, 1 cm.

culture platform. To investigate the characteristics of the muscle tissues in the MuMuTA, we evaluated their morphology and contractile performance. During the culture process, tissue diameter decreased (Fig. 2A), indicating the increase in cell density by the fusion of myoblasts and the successful formation of muscle tissue in our culture process. In addition, immunostaining of the muscle tissues after 8 days of culture revealed striped patterns of α-actinin and actin in the myotubes (Fig. 2B), confirming the formation of sarcomeres, contractile elements of myotubes (*29*). Furthermore, standardized brightness values were calculated with a high-speed Fourier transform for actin-stained images to estimate the distribution of myotubes (*26*, *30*, *31*), showing that the myotubes were oriented roughly in the same direction (Fig. 2C). These results indicate that muscle tissues with mature and aligned myotubes can be formed with our methods.

As the evaluation for the contractile performance of muscle tissue, we investigated how contractile force changes with culture period, tissue length, and electrical stimulation conditions. As a result, the contractile force was greater in the 8-day culture compared with the 12-day and 16-day cultures, and it became even greater by the 20-day culture (Fig. 2D). We speculate that the muscle tissues reached a certain degree of maturity by day 8, with progressive maturation continuing until day 20. Given the lack of a significant difference in contractile

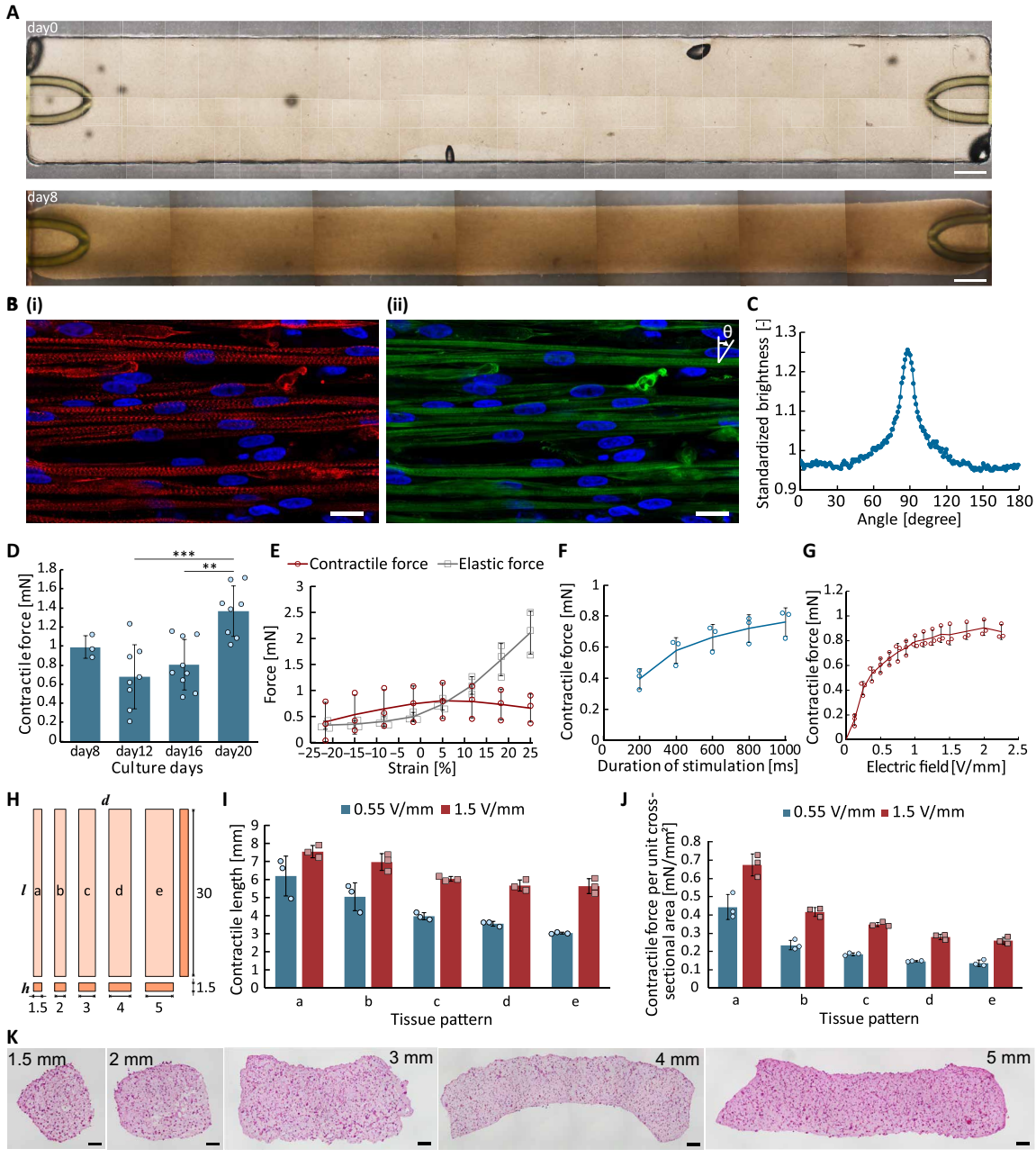

Fig. 2. Evaluation of muscle tissues constructed and cultured on our devices. (**A**) Microscopic images of human skeletal muscle tissue. At day 0, the tissue was inside the PDMS mold. At day 8, the tissue was on the MuMuTA culture platform. Scale bars, 1 mm. (**B**) Immunostaining images of muscle tissues. Red, α-actinin; green, F-actin; blue, cell nuclei. Scale bars, 20 μm. (**C**) Directional distribution of brightness of muscle fibers in the muscle tissue shown in the immunostaining image [(B), ii] calculated by fast Fourier transform. (**D**) Contractile force characteristics of different muscle tissues ($n > 3$) at different culture days. Significance was determined with the Tukey's post hoc test (**$P < 0.01$; ***$P < 0.001$). (**E**) Force-length relationship of different muscle tissues ($n = 3$). (**F**) Changes in contractile force of different muscle tissues ($n = 3$) under different stimulation durations. (**G**) Changes in contractile force of different muscle tissues ($n = 3$) under different voltages of electrical pulses. (**H**) Schematic representation of the dimensions of five kinds of muscle tissues. (**I**) Contractile lengths of different muscle tissues ($n = 3$) with different dimensions. (**J**) Values of the contractile force per unit cross-sectional area of different tissues ($n = 3$) with different dimensions. (**K**) Cross-sectional images of muscle tissues stained with H&E. Scale bars, 100 μm. Data represent means ± SD.

force between the 8-day and 20-day cultures, we chose the 8-day culture for its shorter production time. Moreover, the maximum contractile force was generated when the muscle tissues were stretched to 5% of their length, with the elastic force gradually increasing with further stretching (Fig. 2E). This suggests that our muscle tissues exhibited a length-force relationship similar to that of living muscle (*32*). In addition, the contractile force increased with the duration and voltage of electrical stimulation, saturating at 600 ms and 1.5 V/mm, respectively (Fig. 2, F and G), similar to the changes in contractile force relative to electrical pulses seen in conventional muscle tissues

(*33*, *34*). These results also suggest that the contractile force can be modulated by adjusting the parameters of electrical stimulation.

To investigate whether high-voltage stimulation would damage the muscle tissues and decrease contractile performance, we continuously applied 2-ms electrical pulses at 1.5 V/mm for 600 ms every 3 s to the muscle tissues. Initially, the contractile force increased slightly within the first minute, followed by a gradual decline. After 10 min, the contractile force became ~90% of the initial value (fig. S3A). However, after resting the muscle tissues for 1 hour and then reapplying electrical stimulation, the contractile force recovered to the initial value (fig. S3B). In living muscles, the reversible decline in performance during activity with recovery that mostly happens in the first hour is usually defined as muscle fatigue (*35*). Therefore, the results above indicate that continuous high-voltage stimulation only leads to muscle fatigue without substantial tissue damage. In addition, from periodic measurements of the contractile distance under electrical stimulation of the long-term cultured muscle tissues, we confirmed that, although the muscle tissue can contract up to day 178 of culture, the contractility gradually decreased (fig. S4). This result indicates that the incubation period of 1 to 3 weeks is appropriate for the muscle tissue. Moreover, although the contractile force of muscle tissue decreased by about half at a lower temperature (4°C), the muscle still maintained contractile force in room temperature (26°C) medium as it did in 37°C medium (fig. S5), suggesting that muscle tissue is available in the laboratory for short periods.

We hypothesized that a MuMuTA would outperform a single thicker muscle tissue of equivalent total cross-sectional area. To validate this, we created five types of muscle tissues with widths of 1.5, 2, 3, 4, and 5 mm, all of the same length and thickness (Fig. 2H). Their contractile lengths during the electrical stimulation were compared, revealing that thinner muscle tissue exhibited a greater contractile length (Fig. 2I). Furthermore, we measured the contractile forces of these tissues and calculated the contractile force per unit cross-sectional area using the measured cross-sectional area from optical coherence tomography (OCT) imaging (fig. S6). The contractile force per unit cross-sectional area increased as the muscle tissue became thinner (Fig. 2J). The results suggest that a muscle bundle composed of thinner muscle tissues will exhibit greater contractile force and contractile length compared with a single thicker muscle tissue. In addition, we observed the cross-sectional view of these five types of tissues after hematoxylin and eosin (H&E) staining and did not find any notable necrosis or changes in cell density (Fig. 2K).

Driving properties of MuMuTAs

We varied culture methods, the number of muscle tissues, and electrical stimulation conditions to investigate the contractile performance of MuMuTAs. Given that MuMuTAs were formed by rolling a MuMuSheet into a three-dimensional (3D) structure, it was transformable between a sheet-like configuration and a rolled 3D form. To assess the benefits of this structural transformation, we compared two culture methods: "in-sheet" culture, where the MuMuSheet was rolled before being used as a MuMuTA after culturing on the MuMuTA culture platform, and "in-bundle" culture, where the MuMuSheet was rolled and cultured in the rolled form. Measurement of contractile forces showed that MuMuTAs from the in-sheet culture exhibited stronger contractile force than those from the in-bundle culture (Fig. 3A). This result suggests that the in-sheet culture supports better muscle tissue growth with sufficient oxygen and nutrient supply because all muscle tissues have the same short distance from the liquid surface. In the case of the in-bundle culture, the liquid level was higher than that of the in-sheet culture to cover all muscle tissues. Because the concentration of oxygen decreases as the depth of the culture liquid deepens (*36*, *37*), the muscle tissues on the lower side did not get the same sufficient oxygen, leading to a larger individual difference in muscle tissues and a decrease in the overall contractile force of the MuMuTA.

The design of the MuMuTA allowed an adjustable incorporation of up to eight muscle tissues. We measured the overall contractile force according to the tissue number in the MuMuTA. Increasing the tissue number enhanced the contractile force of the MuMuTA (Fig. 3B), demonstrating the possibility of controlling the overall output force of the MuMuTA by adjusting the tissue number. In addition, variations in electrical stimulations also affected the contractile performance of the MuMuTA. The contractile force of the MuMuTA increased with the increase in the duration and voltage of electrical pulses, reaching ~8 mN as the near saturation value at 600-ms duration and 1.5-V/mm electric field (Fig. 3, C and D), and maintained its maximum contractile force for ~30 min of continuous operation (fig. S7). Moreover, to investigate the relationship between contractile length and electrical stimulations, we placed electrodes diagonally on the sides of the vertically suspended MuMuTA to stimulate it (fig. S8) and measured the distance traveled at the bottom of the MuMuTA (Fig. 3E). The contractile length of the MuMuTA increased with the voltage, reaching ~4 mm at 1.5 V/mm (Fig. 3F). These results demonstrate that the MuMuTA can control the contractile force within a relatively larger range than single muscle tissue. Unlike a single tissue whose contraction can be regulated only by electrical stimulation conditions, the overall output force of the MuMuTA can be regulated by varying the number of muscles, thus providing control with more gradients.

Moreover, the MuMuTA achieved partial contraction through selective stimulation, providing three–degrees-of-freedom (3-DOF) actuation. We selectively stimulated the muscle tissues within the vertically suspended MuMuTA by controlling the position of the electrodes. The MuMuTA succeeded in rotations of its bottom part in the roll and pitch directions, as well as vertical movements (fig. S9 and movie S1). Given that only vertical movements were required to actuate biohybrid fingers, the electrodes were aligned to the long axis of the muscle tissues to ensure uniform stimulation of each muscle tissue in the MuMuTA.

Performance of a biohybrid finger powered by a MuMuTA

Before assembling the biohybrid hand, we tested the performance of single biohybrid fingers. The contraction of a MuMuTA aroused by the electrical stimulation pulled the tendon-like structure and caused finger flexion (Fig. 4A). By tracking the angle changes at each joint, we confirmed that the first, second, and third joints of the finger sequentially rotated and reached angles ranging from 20° to 60° (Fig. 4B and fig. S10A). The total rotation angle sum of the three joints reached ~130°, and the angular velocity was up to nearly 500°/s for a single joint (fig. S10B). This result demonstrates that the MuMuTA has sufficient contractile force and length to overcome friction and enable effective cable-driven actuation.

Furthermore, we investigated the changes in the total angle (sum of the angles of the three joints) of biohybrid fingers at different voltages (Fig. 4C). The peak total angle during the actuation increased with higher voltage, showing the controllability of

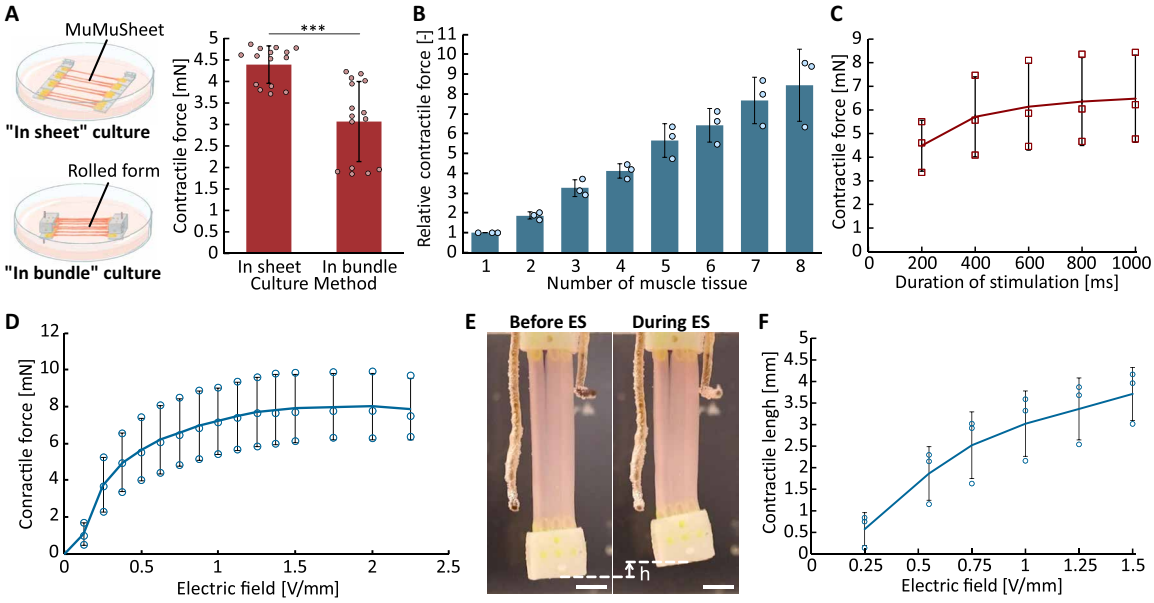

Fig. 3. Evaluation of MuMuTA properties. (**A**) Comparison of contractile forces of different contractions of MuMuTAs ($n = 15$) produced under two culture methods. Significance was determined by Student's t test (***$P < 0.001$). (**B**) Variations in the overall contractile forces of different MuMuTAs ($n = 3$) when the number of muscle tissues within the MuMuTA was changed, relative to having only one muscle tissue. (**C**) Changes in the contractile forces of different MuMuTAs ($n = 3$) under different stimulation durations and (**D**) different stimulation voltages. (**E**) Image of the MuMuTA suspended in the transparent culture medium, with the bottom moving upward when subjected to electrical stimulation. Scale bars, 5 mm. (**F**) Changes in the contractile lengths of different MuMuTAs ($n = 3$) under different stimulation voltages. The contractile length is represented by "h" in (E). Data represent means ± SD.

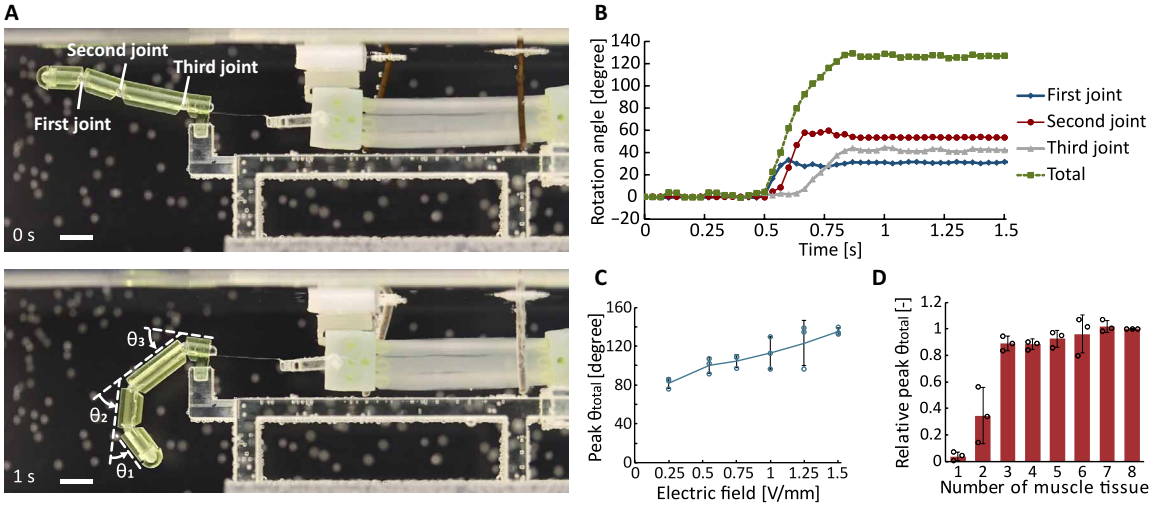

Fig. 4. Performance evaluation of a biohybrid finger driven by a MuMuTA. (**A**) Image of a biohybrid finger before and after applying electrical stimulation. Scale bars, 5 mm. (**B**) Angular changes in joints over time. The rotation angle represents the change in joint angles, and "total" indicates the sum of the three joints. The rotation angles are zero in the initial state before the actuation of the MuMuTA. (**C**) Variation in the peak total angle ($\theta_{total} = \theta_1 + \theta_2 + \theta_3$) of different biohybrid fingers ($n = 3$) during electrical stimulation under different voltages. (**D**) Changes in the peak total angle of different fingers ($n = 3$) relative to having only one muscle tissue when the number of muscle tissues within the MuMuTA was altered. Data represent means ± SD.

biohybrid finger motions via muscle contractions. In addition, when the MuMuTA had only one muscle tissue, the finger hardly rotated (Fig. 4D). With two muscle tissues, the finger could reach only 40% of the maximum angle when driven by the MuMuTA with eight muscle tissues. On the other hand, when the MuMuTA had three or more muscle tissues, its contractions achieved the rotation of the finger with a nearly maximum angle. The result suggests that the MuMuTA with only three muscle tissues can already provide sufficient contractile force to overcome joint friction and allow the finger to reach an angle close to the maximum angle. The reversibility and repeatability of the finger rotation depended on the peak total angle reached during the actuation (fig. S10, C and D). When the finger rotated back slightly because of buoyancy after one stimulation, the finger could still reach a similar angle as the first

stimulation during subsequent stimulations (fig. S10E). These results indicate that the MuMuTAs have suitable drive characteristics for continuous finger movements.

Performance of the biohybrid hand with five fingers

Applying electrical pulses to all MuMuTAs induced all fingers to flex simultaneously (Fig. 5, A to C, and movie S2). Stimulating only a specific MuMuTA caused the corresponding finger to bend individually with minimal influence on other fingers (Fig. 5D and movie S3). Using these driving characteristics, we applied electrical stimulation sequentially at 500-ms intervals from the little finger to the thumb, resulting in sequential finger flexion (Fig. 5E and movie S4). These results demonstrate the ability to individually operate the fingers of the biohybrid hand, enabling complex movements. Simulating the electric field distribution with and without glass walls at the forearm part confirmed that the glass walls effectively contributed to individual finger operation (figs. S11 and S12). To demonstrate the capabilities of the biohybrid hand, we simultaneously activated the little finger, ring finger, and thumb, causing the biohybrid hand to form a scissors gesture (Fig. 5F and movie S5). Moreover, the biohybrid hand not only could perform complex postures but also could manipulate objects. We placed a pipette tip under the fingers in the initial position of the biohybrid hand and applied the electrical stimulation to all MuMuTAs. The flexion of the fingers caused the tip to move, demonstrating that the biohybrid hand has an object-manipulating ability (Fig. 5G and movie S6). These abilities to flex multijointed fingers, control each finger separately, and manipulate objects make it possible for our biohybrid hand to realize many complex movements, thus contributing to the mimicry of a living hand.

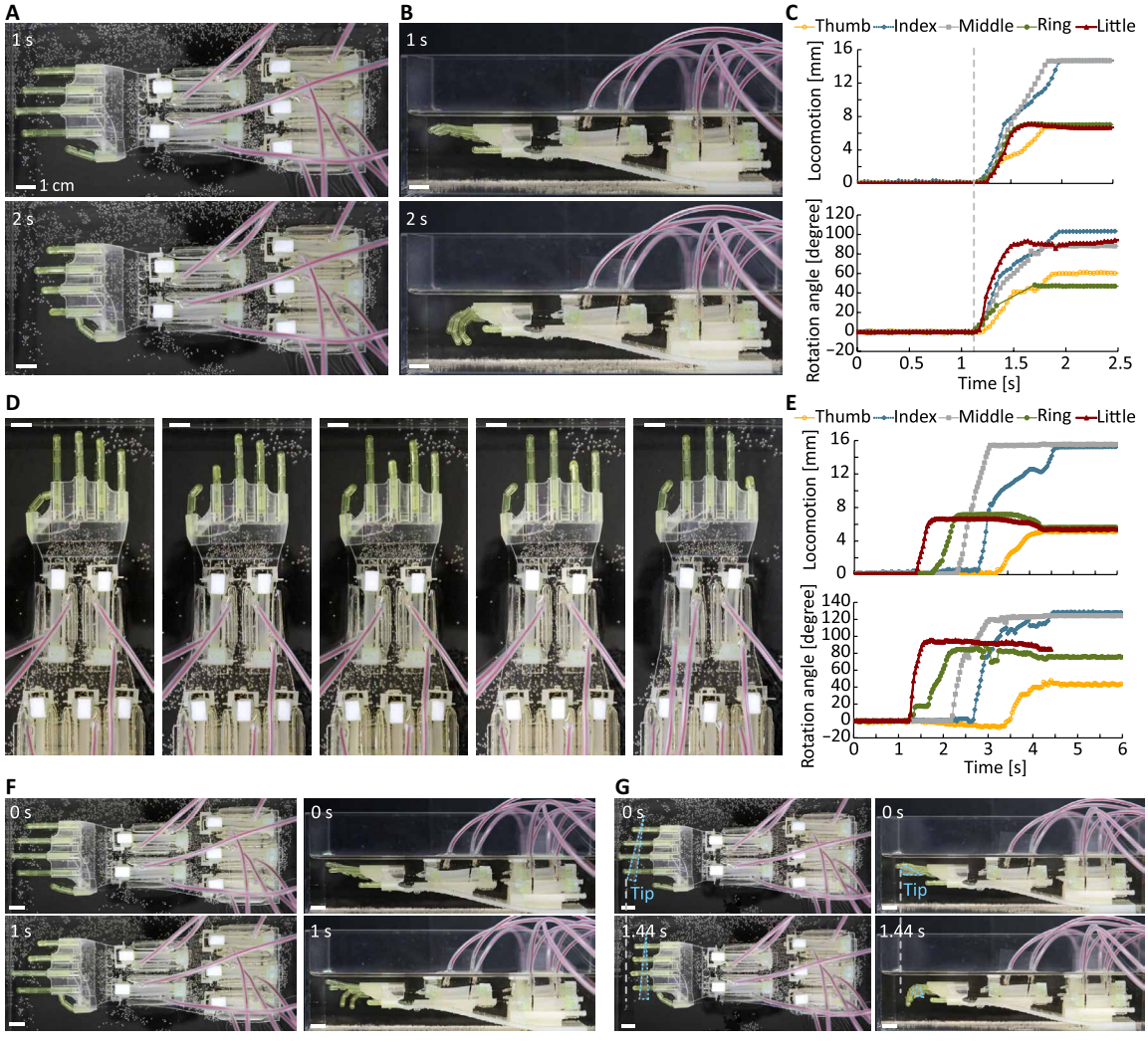

Fig. 5. Performance evaluation of the biohybrid hand driven by MuMuTAs. (**A** and **B**) (A) Top view images and (B) side view images of the biohybrid hand before and after simultaneously stimulating five MuMuTAs. Scale bars, 1 cm. (**C**) Changes in fingertip displacement and total rotation angles of the five fingers when simultaneously stimulating five MuMuTAs. (**D**) State of the biohybrid hand after individually stimulating each MuMuTA. From left to right, each MuMuTA corresponding to the thumb to the little finger was individually stimulated. Scale bars, 1 cm. (**E**) Changes in fingertip displacement and total rotation angle of the five fingers when sequentially activating the corresponding MuMuTA from the little finger to the thumb. (**F**) Top view and side view images of the biohybrid hand performing a scissors gesture when simultaneously stimulating the thumb, ring finger, and little finger. Scale bars, 1 cm. (**G**) Manipulation of the tip with the biohybrid hand when simultaneously stimulating all MuMuTAs. The tip moves under the influence of finger flexion. Scale bars, 1 cm.

DISCUSSION

This study proposed the MuMuTA composed of multiple skeletal muscle tissues. Using the MuMuTA, we successfully implemented a cable-driven mechanism to bend a multijointed finger through muscle contraction. We finely controlled the rotation of the finger by adjusting the output force of the MuMuTA. In addition, we demonstrated the drive of a biohybrid hand with five fingers, enabling the individual control of fingers and the manipulation of objects. These results show that the MuMuTA has sufficient contractile force and length to drive a multilink mechanism and can control the output within a relatively large range.

The sushi roll–like method for MuMuTA allowed multiple muscle tissues to be cultured in a sheet form, generating better contractility than that of muscle tissue cultured in a bundle form. This method allowed the MuMuTA to be formed from the MuMuSheet just before use and to be returned to the MuMuSheet after use, avoiding the culture in the bundle form that causes the degradation of contractility. In addition, further improvements in the contractility of the MuMuTA can be expected. The current MuMuTA can contain eight skeletal muscle tissues; however, by increasing the density of the tissue arrangement, more muscle tissues could be included in the same space, allowing larger contractile force to be generated from the same size MuMuTA. Furthermore, by increasing the number and length of muscle tissues, along with corresponding upgrades to the design of the anchor holder, a larger and more powerful MuMuTA could potentially be realized. However, certain practical factors, such as the number of cells required and the size of the culture space, may limit the further scaling up of MuMuTAs.

There is room for improvement in the construction of the biohybrid hand. Now, the float keeps the MuMuTA's contractile movements parallel to the liquid surface without friction but only in the horizontal direction. Once guides are mounted to the anchor holders and MuMuTAs can exert enough contractile force to ignore the friction of the guides, the biohybrid hand facing in any direction can be usable in the future. In addition, the current fingers are difficult to return to their initial position after being stimulated once because the restoring force is only provided by buoyancy. To achieve continuous movements of the biohybrid hand, it is essential to enable the fingers to return to their initial positions after electrical stimulation automatically. To solve this issue, an elastic material opposing the motion controlled by the MuMuTA needs to be introduced. Ideally, this elastic material should provide minimal resistance during MuMuTA contraction and sufficient restoring force for returning the finger to its original position during MuMuTA relaxation. However, finding a suitable elastic material and designing such a system may pose challenges. Another approach involves introducing five additional MuMuTAs that act in opposition to the existing ones, like the finger extensor apparatus in human hands (*38*). Connecting these opposing MuMuTAs to the back of the fingers makes it possible to straighten the fingers by contracting the opposing MuMuTAs. Moreover, improving the contractility of the muscle tissues in the MuMuTA is crucial. Although the contractile force per unit area of our cultured muscle (0.7 mN/mm^2) is still lower than that of living muscle, such as the 6 mN/mm^2 observed in 12- to 15-week-old fetal muscle (*39*), it is expected that the contractility can be enhanced through physical training (*40*) and the addition of growth-promoting chemical factors (*41*). In addition, to make our biohybrid hand more similar to a human hand, lateral movement of the fingers also needs to be achieved. By replacing the third joint of the finger with a ball joint and introducing some mechanical design for using the 3-DOF motion of the MuMuTA, the finger could rotate laterally. These future modifications will allow actions like pinching a pencil between two fingers.

Together, these findings show that the MuMuTA serves as an effective driving source for biohybrid robots and holds notable potential in biohybrid robotics, providing substantial contractile force and length and serving as an in vitro dynamic model for muscle contractions. This successful development marks a milestone for advancing large-scale biohybrid robots. Until now, muscle-driven robots have been limited to small sizes with simple structures. One major goal of biohybrid robots is to mimic biological systems, which necessitates scaling up their size and achieving high power output and major actuation. The key achievement lies in creating actuators from bundled thin muscle tissues that can survive long term without necrosis while producing substantial power and displacement. This design principle will enable the construction of larger and more complex robots in the future. In addition, the use of human myoblasts in the MuMuTA suggests its potential as a drug-testing model using contractility as an evaluation index (*42*–*44*) and a dynamically exercisable model coculturing with motor neurons (*45*–*47*). Therefore, we believe the MuMuTA and the biohybrid hand will be valuable tools across various applications, from engineering to medicine.

MATERIALS AND METHODS

Cell preparation

The cells used were prescreened human skeletal muscle cells (Cell Applications Inc.) with fewer than three passages. We cultured the myoblasts in skeletal muscle cell growth medium-2 (SkGM-2, Lonza) at 37°C in a 5% CO_2 atmosphere. After cell proliferation, we peeled off the cells in the following process for single-cell suspensions (2×10^5 to ~4×10^5 cells/ml). After removing the growth medium from the petri dishes, we washed the adherent cells twice with phosphate-buffered saline (-) [PBS (-)]. Each petri dish was filled with 1 ml of trypsin-EDTA and placed in the incubator for 3 min. After the cells were detached, we added 9 ml of growth medium to each petri dish. The cell suspension was homogenized by pipetting and transferred to a centrifuge tube.

Fabrication of the anchor holder

The parts of the anchor holder were fabricated with a stereolithography machine (DigitalWax 028J, Sea Force Co. Ltd.). We deposited a 2-μm-thick layer of parylene C on the surface of the parts to improve their biocompatibility and a 5-μm-thick layer on a glass plate to make the parylene sheet using a chemical vapor deposition machine (SCS PDS 2010 Labcoter, Specialty Coating Systems Inc.). For the parylene sheet to wrap around and hold the parts of the anchor holder without breaking, a distance between the parts of the anchor holder was needed according to their thickness (fig. S2B). On the basis of microscope photographs (fig. S2C), we set up a 450-μm distance between the parts (fig. S2D). We applied a liquid photopolymer (Norland Optical Adhesive 63) between the parts and a parylene sheet cut from the glass plate and cured the liquid photopolymer with a laser machine (UV-400, Keyence Corp.). Two micrometers of parylene C was deposited again on the surface of the connected part to prevent the photopolymer from making direct contact with the culture medium and to make the connections stronger.

Formation and culture of multiple muscle tissues

As the culture device for human skeletal muscle tissues, we fabricated the anchors with a 3D printer (microArch S140, BMF) and deposited

2 μm of parylene C and fibronectin (0.1 mg/ml in PBS) on the surface of the anchors. In addition, we shaped PDMS molds in resin casts fabricated with a 3D printer (Agilista, Keyence Corp.). To prevent the cells and the hydrogel from adhering to the PDMS molds, we coated the PDMS molds using 2-methacryloyloxyethyl phosphorylcholine polymer solution (0.5 wt % Lipidure-CM5206 in 99% ethanol) and bovine serum albumin (BSA) solution (1% BSA in PBS). All devices were ultraviolet and ozone sterilized and washed three times with PBS before the experiments.

We embedded the anchors inside the PDMS molds (fig. S13A) and poured hydrogel solution into the molds (fig. S13B). The hydrogel solution was composed of Matrigel, the growth medium, fibrinogen, thrombin, and myoblasts (1.5×10^7 cells/ml). We put the samples into the incubator for 30 min to gel the hydrogel (fig. S13C) and cultured striped structures of myoblast-laden hydrogel in the growth medium with 1% amino caproic acid (ACA) for 2 days (fig. S13D).

The MuMuTA culture platform was composed of a PDMS base (fabricated with the same method as the PDMS mold), a pair of anchor holders, and a 3D-printed stopper (formed with Agilista printer) to fix the anchor holders. We assembled the devices in the petri dish and put differentiation medium composed of Dulbecco's modified Eagle's medium (DMEM) (low glucose) with 1% ACA, 2% horse serum, penicillin (100 U/ml), streptomycin (100 μg/ml), recombinant human IGF-1 (insulin-like growth factor 1) (10 ng/ml; PeproTech), and 5 μM SB431542 (Cayman Chemical) in the dish. Then, we moved the striped structures of myoblast-laden hydrogel from the PDMS molds to the MuMuTA culture platform (fig. S13E) and cultured them in the incubator to form the muscle tissues (fig. S13F).

Immunostaining

To examine the maturity and orientation of muscle fibers, we fixed the muscle tissues and stained α-actinin, cytoskeleton (F-actin), and cell nuclei. In the immunostaining α-actinin, the reagents used were a primary antibody (monoclonal anti–α-actinin antibody, Sigma-Aldrich) and a secondary antibody (goat anti-mouse immunoglobulin Alexa Fluor 568, Thermo Fisher Scientific). F-actin was stained with phalloidin (Alexa Fluor 488, Thermo Fisher Scientific). Cell nuclei were stained with DAPI (4′,6-diamidino-2-phenylindole, Invitrogen).

For the staining, muscle tissues were washed three times with PBS to remove the serum component. Then, they were fixed by adding 4% paraformaldehyde (PFA) and left at room temperature for 20 min. After the tissues were washed three times with PBS, 0.3% Triton X-100 was added for 20 min at room temperature to facilitate cell permeabilization. They were then washed three times with PBS. Next, the tissues were blocked by adding 2.5% BSA and left overnight at 4°C. The tissues were cultured with the primary antibody and phalloidin overnight at 4°C (primary antibody was used at a 1/1000 dilution, and phalloidin was used at a 1/500 dilution). After washing the samples three times with PBS, we added the secondary antibody and left them at room temperature for 105 min. Then, DAPI (1 μg/ml) was added, and the samples were left for 15 min, followed by washing three times with PBS.

Cross-sectional image of muscle tissues

To observe the cross section of muscle tissues and assess the extent of necrosis, we prepared tissue sections and visualized them by an H&E staining method. After fixing the muscle tissues using the same method mentioned above, we sequentially immersed the tissues overnight subsequentially in 30, 50, and 70% sucrose solutions at 4°C. Next, the tissues were frozen using liquid nitrogen after being soaked in an optional cutting temperature compound (OCT compound, Sakura Finetek Japan Co. Ltd.) overnight. Tissue sections with a thickness of 8 μm were obtained using a cryostat (NX50, Thermo Fisher Scientific) and attached to glass slides (MAS coated glass slide, Matsunami Glass Ind. Ltd.). The sections were then subjected to H&E staining. First, the glass slides were immersed in water for 5 min twice to remove the OCT compound. Then, they were immersed in hematoxylin for 5 min, followed by a 5-min rinse in water to remove excess hematoxylin. Afterward, the sections were immersed in eosin for 5 min, followed by three rinses in ethanol for washing and three 5-min rinses in xylene. Mounting medium [Organo (Limonene) Mount, Immuno-BioScience Corp.] was applied to each glass slide, and a cover glass was placed on top. The mounting medium was allowed to diffuse naturally. The stained tissue sections were observed under a microscope (THUNDER Imaging Systems, Leica Microsystems). In the case of imaging the cross section of the muscle tissues without their fixation using PFA, we used an OCT machine (IVS-2000-HR-6, Santec OIS Corporation).

Construction of the MuMuTA

During the rolling process of constructing the MuMuTA (fig. S13G), to roll the pair of anchor holders together, we stuck rectangular glass sticks simultaneously in the U-shaped part of each anchor holder. Then, we mounted a pair of disks with a square hole in the center on the sides of the rectangular glass stick so that we could turn the disks to roll the rectangular glass stick, allowing the MuMuSheet to be rolled. These auxiliary tools helped us roll the pair of anchor holders simultaneously and avoid direct contact with anchor holders or muscle tissues to reduce the risk of contamination. After the rolling process, we pulled out the rectangular glass stick from the side of the anchor holder and fixed the rolled-up MuMuSheet by thrusting two 3D-printed rods (fabricated by DigitalWax printer) into the side holes of the rolled-up anchor holders. Last, the MuMuTA was constructed.

Muscle tissue type and electrical stimulation condition

The muscle tissues constructed with a cross section of 4 mm by 1.5 mm ("tissue d" shown in Fig. 2H) were primarily used in this study, except in the experiments for the comparison of the MuMuTA culture methods, the 3-DOF actuation, and the long-term culture of the muscle tissue. In these experiments, tissues constructed with a cross section of 1.5 mm by 1.5 mm ("tissue a" shown in Fig. 2H) were used.

In all experiments, gold wires with a diameter of 1 mm were used as electrodes, but the condition of the electrodes varied depending on the experiment. In the force-sensing experiment and the experiment of powering the biohybrid finger, the gold electrodes were put directly into the culture medium. In the experiment of powering the biohybrid hand, we connected 10-mm gold electrodes to red conductive wires with a conductive adhesive (Dotite D-723S, FUJIKURA KASEI Co. Ltd.) and then waterproofed the wires by covering them with silicon tubes. In the experiment for contractile length measurement and the 3-DOF actuation, we wrapped the gold wires with parafilm to create insulating parts, allowing only 3 and 10 mm for each experiment, respectively, at the end of the gold wires to be exposed to the culture medium as an electrode.

We used alternating positive and negative electrical pulses as a basic signal to stimulate the muscle tissues. The muscle tissue

condition and the parameters of electrical stimulation are shown in table S1.

Force sensing of the single muscle tissue and the MuMuTA

We assembled a force-sensing system (fig. S14A) for both single muscle tissues (fig. S14B) and MuMuTAs (fig. S14C). The devices used for electrical stimulation included a function generator (Agilent Technologies) to generate the electrical pulses, a high-speed bipolar amplifier (HAS4101, NF Corporation) to amplify the signal, and gold electrodes to stimulate the target sample. The devices used for measurement included a force sensor (T131, TECH ALPHA), a capacitive gauge (P210, TECH ALPHA), a data logger (NR-600, Keyence), and a computer. In addition, we also prepared a 3D-printed reservoir and an L-shaped arm (fabricated by Agilista printer).

The force sensor was turned on for 1 hour before the experiment for preheating, and DMEM high glucose (Fujifilm) with 1% penicillin/streptomycin was warmed and put into the reservoir. When the target sample was electrically stimulated, it contracted and pulled the L-shaped arm, thus pulling the sensing part of the force sensor and causing a change in the internal electrical capacitance of the force sensor. The contractile force of the sample was determined from the variation in the output voltage waveform from the capacitive gauge connected to the force sensor. To reduce error, we took the average of the peak-to-peak values of the waveforms of five cycles of stimulation as the final result. The elastic force was calculated by subtracting the measured output voltage without applying electrical stimulation to the tissue from the initial value of the output voltage taken by inserting an anchor without muscle tissue into the L-shaped arm fixed on the force sensor.

In the experiment testing the contractile force depending on temperature, we placed the medium in 37° and 30°C water baths, a 26°C room temperature environment, and a 4°C refrigerated environment for sufficient time to allow the medium to reach the same temperature as its surroundings. After placing the medium and the muscle tissue in the reservoir, we immediately measured its contractile force.

For the MuMuTA durability test, we paused stimulation every 10 min, replaced the medium in the reservoir with fresh prewarmed medium, and then continued stimulation. We took the average of five peak-to-peak contractions at the start of stimulation as the contractile force at 0 min. For the contractile forces at 10 to 90 min, we averaged the five peak-to-peak values measured at the end of each respective time interval.

Contractile length of the single muscle tissue and the MuMuTA

To measure the contractile length, we hung the single muscle tissue and the MuMuTA separately in a transparent culture medium [DMEM (high glucose) with L-glutamine and Hepes, Fujifilm] using 3D-printed shelves (fabricated by Agilista printer). We hung one end of the samples on devices for fixing and allowed the other end to hang freely under the influence of gravity. When the electrical pulses were applied to the samples, the locomotion of their free ends was recorded with a digital camera (Canon EOS Kiss X10i). We tracked the motion of the free ends using analysis software (VW-9000 MotionAnalyzer, Keyence) to obtain the motion trajectory and the contractile length.

In the long-term culture of the muscle tissues, their contractions were recorded when electrical stimulations were applied. The above software was used to track the movement of reference points on the muscle tissues, and the difference in distance from the initial position was defined as the contractile distance.

Fabrication of the cable-driven robot fingers

The cable-driven robot finger consisted of a multijointed finger skeleton, a tendon-like structure, and a 3D-printed hanger (fabricated with an Agilista printer). The finger skeletons were fabricated using the BMF photolithography machine mentioned earlier (fig. S15A). The finger skeletons had a hollow structure and a removable cap at the tip of the finger, and guide rails for the tendon-like structure were on the inner wall.

For the tendon-like structure of the finger, a 5-μm-thick, 1-mm-wide parylene sheet (the same fabrication methods of the parylene sheet used in the anchor holder mentioned earlier) was used. One side of the parylene sheet was attached to a glass capillary with an outer diameter of 0.3 mm, and the other side was attached to the finger cap (fig. S15B, i). The glass capillary was inserted into the finger from the hole on the fingertip, thus allowing the parylene sheet to pass through the hollow finger skeleton (fig. S15B, ii). Then, we closed the cap to let the parylene sheet be positioned on the inner side of the finger's flexion. The parylene sheet was then removed from the glass tube and attached to the hanger (fig. S15B, iii). Last, we obtained the cable-driven robot finger (fig. S15C).

Assembly of the biohybrid finger and biohybrid hand

A biohybrid finger consisted of a cable-driven robot finger, a MuMuTA, and a float (fig. S15D). We attached a styrene board to a 3D-printed part (fabricated by Agilista printer) that could be fixed on the rolled anchor holder to make a float. We fixed one side of the MuMuTA on a ring-shaped holder (3D-printed with an Agilista printer) and hung the hanger of the robot finger onto the other side of the MuMuTA. After setting the float on the anchor holder linked to the robot finger, we adjusted the position of the ring-shaped holder and the amount of the transparent culture medium to align the MuMuTA and tendon-like structure to form a straight line, thereby increasing the efficiency of using the actuation of the MuMuTA. A pair of gold electrodes was placed diagonally on the sides of the MuMuTA to apply the electrical stimulation.

A biohybrid hand consisted of five biohybrid fingers and a hand substrate with a shape mimicking a human hand (fig. S15E, i). Each biohybrid finger was designed with a different position in the transparent culture medium; thus, the length of the tendon-like structure and the size of the float were different from each other (fig. S15E, ii). We assembled the biohybrid hand in the same way as the biohybrid finger (fig. S15F) and mounted the back of the hand after the fingers were fixed. We placed glass walls on both sides of each MuMuTA to suppress the diffusion of the electrical stimulation in the transparent culture medium.

For driving each finger in the biohybrid hand selectively, we made a system to supply the electrical pulses to the respective target MuMuTA. A circuit for transmitting the electrical signals to the MuMuTA was composed of an Arduino Uno, 10 relays (SRD-05VDC-SL-C) for the positive and negative electrodes of five fingers, respectively. A laptop was connected to the Arduino, which transmitted on/off signals to the relays, which, in turn, caused the relay to control the on/off switch of the amplified electrical signals used to stimulate the MuMuTA. Unless otherwise mentioned, when the signal to turn on was sent to the Arduino, alternating positive and negative electrical pulses (2-ms duration) were delivered to the MuMuTAs for 1500 ms. In the experiment of

powering the biohybrid finger and hand, each time before the MuMuTA actuation, we straightened the finger to a near-horizontal initial position with tweezers.

Motion analysis of the biohybrid finger and the biohybrid hand

The camera and tracking software for the motion analysis of the biohybrid finger and hand were the same as those used in the measurement of the contractile length, except that we used two cameras to record the motion of the biohybrid hand both from the top and from the side. The fingertip displacement of the index to the little finger and the total rotation angle of the thumb were tracked using the video from the top, whereas the total rotation angle of the index to the little fingers and the fingertip displacement of the thumb were tracked using the video from the side. In the analysis of the side view, two tracking points were set on each link of the finger, and the relative angles of straight lines formed by the two tracking points of each link were used to determine the angles of each joint of the finger. In the analysis of the top view, we tracked the movements of the fingertips to determine the locomotion.

Simulation for the distribution of an applied electric field

We used a simulation software (COMSOL Multiphysics) to estimate the electric field around the MuMuTAs in the biohybrid hand–driving experiment and force-sensing experiment. We set up a block of material defined as the transparent culture medium for the respective models, and the size of these blocks (200 mm by 100 mm by 40 mm in the model for the biohybrid hand–driving experiment and 83 mm by 56 mm by 13 mm in the model for the force-sensing experiment) was determined on the basis of the size of the containers and the amount of the transparent culture medium in the actual experiments. In the model for the biohybrid-driving experiment, we made an approximation of the forearm part of the actual design of the hand skeleton and mounted five MuMuTAs on it, and the anchor holders of the MuMuTAs and the eight muscles were each approximated as similarly sized blocks as well (7.7 mm by 8.5 mm by 8.5 mm for the anchor holder and 30 mm by 1.5 mm by 1.5 mm for the muscle tissue). A pair of gold electrodes and glass walls (only in the model with glass walls) were mounted on both sides of the MuMuTAs, and one of the electrodes was assigned the desired voltage whereas the other electrode was set to 0 V (fig. S11). The electrodes were set up in the same way in the model for the force-sensing experiment. The conductivity and the relative permittivity of the material used in the simulation are listed in table S2. We calculated the volume integration of the electric field intensity within all muscle tissues in the MuMuTA (VI_E) (*48*) to investigate how much the muscle tissues would be stimulated with different voltages and configurations of the experimental setup.

Statistical analysis

All error bars represent SDs. In the significance test of comparison of the contractile forces of MuMuTAs using different culture methods, we first used an F test to determine whether the variances of the two populations were equal, and on the basis of the result, we then used Student's two-sample t test assuming equal variances to calculate the significant difference. Other significance tests used Tukey's post hoc test.

Supplementary Materials

The PDF file includes:
Figs. S1 to S15
Tables S1 and S2

Other Supplementary Material for this manuscript includes the following:
Movies S1 to S6
MDAR Reproducibility Checklist

REFERENCES AND NOTES

1. W. R. Frontera, J. Ochala, Skeletal muscle: A brief review of structure and function. *Calcif. Tissue Int.* **96**, 183–195 (2015).
2. M. T. Lam, Y. C. Huang, R. K. Birla, S. Takayama, Microfeature guided skeletal muscle tissue engineering for highly organized 3-dimensional free-standing constructs. *Biomaterials* **30**, 1150–1155 (2009).
3. S. Hinds, W. N. Bian, R. G. Dennis, N. Bursac, The role of extracellular matrix composition in structure and function of bioengineered skeletal muscle. *Biomaterials* **32**, 3575–3583 (2011).
4. L. J. Rao, Y. Qian, A. Khodabukus, T. Ribar, N. Bursac, Engineering human pluripotent stem cells into a functional skeletal muscle tissue. *Nat. Commun.* **9**, 126 (2018).
5. Y. J. Choi, Y. J. Jun, D. Y. Kim, H. G. Yi, S. H. Chae, J. Kang, J. Lee, G. Gao, J. S. Kong, J. Jang, W. K. Chung, J. W. Rhie, D. W. Cho, A 3D cell printed muscle construct with tissue-derived bioink for the treatment of volumetric muscle loss. *Biomaterials* **206**, 160–169 (2019).
6. E. van der Wal, A. Iuliano, S. L. M. In't Groen, A. P. Bholasing, D. Priesmann, P. Sharma, B. den Hamer, V. Saggiomo, M. Krüger, W. W. M. P. Pijnappel, J. C. de Greef, Highly contractile 3D tissue engineered skeletal muscles from human iPSCs reveal similarities with primary myoblast-derived tissues. *Stem Cell Reports* **18**, 1954–1971 (2023).
7. L. Ricotti, B. Trimmer, A. W. Feinberg, R. Raman, K. K. Parker, R. Bashir, M. Sitti, S. Martel, P. Dario, A. Menciassi, Biohybrid actuators for robotics: A review of devices actuated by living cells. *Sci. Robot.* **2**, eaaq0495 (2017).
8. Y. Morimoto, H. Onoe, S. Takeuchi, Biohybrid robot powered by an antagonistic pair of skeletal muscle tissues. *Sci. Robot.* **3**, eaat4440 (2018).
9. J. C. Nawroth, H. Lee, A. W. Feinberg, C. M. Ripplinger, M. L. McCain, A. Grosberg, J. O. Dabiri, K. K. Parker, A tissue-engineered jellyfish with biomimetic propulsion. *Nat. Biotechnol.* **30**, 792–797 (2012).
10. K. Kabumoto, T. Hoshino, Y. Akiyama, K. Morishima, Voluntary movement controlled by the surface EMG signal for tissue-engineered skeletal muscle on a gripping tool. *Tissue Eng. Part A* **19**, 1695–1703 (2013).
11. G. J. Pagan-Diaz, X. T. Zhang, L. Grant, Y. Kim, O. Aydin, C. Cvetkovic, E. Ko, E. Solomon, J. Hollis, H. Kong, T. Saif, M. Gazzola, R. Bashir, Simulation and fabrication of stronger, larger, and faster walking biohybrid machines. *Adv. Funct. Mater.* **28**, 1801145 (2018).
12. Y. Kim, Y. Yang, X. Zhang, Z. Li, A. Vázquez-Guardado, I. Park, J. J. Wang, A. I. Efimov, Z. Dou, Y. Wang, J. Park, H. W. Luan, X. C. Ni, Y. S. Kim, J. Baek, J. J. Park, Z. Q. Xie, H. B. Zhao, M. Gazzola, J. A. Rogers, R. Bashir, Remote control of muscle-driven miniature robots with battery-free wireless optoelectronics. *Sci. Robot.* **8**, add1053 (2023).
13. R. Raman, L. Grant, Y. Seo, C. Cvetkovic, M. Gapinske, A. Palasz, H. Dabbous, H. Kong, P. P. Pinera, R. Bashir, Damage, healing, and remodeling in optogenetic skeletal muscle bioactuators. *Adv. Healthc. Mater.* **6**, 1700030 (2017).
14. Y. Morimoto, H. Onoe, S. Takeuchi, Biohybrid device with antagonistic skeletal muscle tissue for measurement of contractile force. *Adv. Robot.* **33**, 208–218 (2019).
15. M. Guix, R. Mestre, T. Patiño, M. De Corato, J. Fuentes, G. Zarpellon, S. Sánchez, Biohybrid soft robots with self-stimulating skeletons. *Sci. Robot.* **6**, eabe7577 (2021).
16. H. Tetsuka, L. Pirrami, T. Wang, D. Demarchi, S. R. Shin, Wirelessly powered 3D printed hierarchical biohybrid robots with multiscale mechanical properties. *Adv. Funct. Mater.* **32**, 2202674 (2022).
17. K. Y. Lee, S. J. Park, D. G. Matthews, S. L. Kim, C. A. Marquez, J. F. Zimmerman, H. A. M. Ardona, A. G. Kleber, G. V. Lauder, K. K. Parker, An autonomously swimming biohybrid fish designed with human cardiac biophysics. *Science* **375**, 639–647 (2022).
18. R. Kinjo, Y. Morimoto, B. Jo, S. Takeuchi, Biohybrid bipedal robot powered by skeletal muscle tissue. *Matter* **7**, 948–962 (2024).
19. Y. Morimoto, H. Onoe, S. Takeuchi, Biohybrid robot with skeletal muscle tissue covered with a collagen structure for moving in air. *APL Bioeng.* **4**, 026101 (2020).
20. K. Morita, Y. Morimoto, S. Takeuchi, Biohybrid tensegrity actuator driven by selective contractions of multiple skeletal muscle tissues. *Biofabrication* **15**, 045002 (2023).
21. Z. W. Li, Y. Seo, O. Aydin, M. Elhebeary, R. D. Kamm, H. Kong, M. T. A. Saif, Biohybrid valveless pump-bot powered by engineered skeletal muscle. *Proc. Natl. Acad. Sci. U.S.A.* **116**, 1543–1548 (2019).
22. Z. Yuan, Q. H. Guo, D. L. Jin, P. F. Zhang, W. G. Yang, Biohybrid soft robots powered by myocyte: Current progress and future perspectives. *Micromachines* **14**, 1643 (2023).
23. E. H. Sonnenblick, Series elastic and contractile elements in heart muscle: Changes in muscle length. *Am. J. Physiol.* **207**, 1330–1338 (1964).

24. R. J. Maughan, J. S. Watson, J. Weir, Strength and cross-sectional area of human skeletal-muscle. *J. Physiol.* **338**, 37–49 (1983).
25. Y. Morimoto, S. Mori, F. Sakai, S. Takeuchi, Human induced pluripotent stem cell-derived fiber-shaped cardiac tissue on a chip. *Lab Chip* **16**, 2295–2301 (2016).
26. Y. Morimoto, M. Kato-Negishi, H. Onoe, S. Takeuchi, Three-dimensional neuron-muscle constructs with neuromuscular junctions. *Biomaterials* **34**, 9413–9419 (2013).
27. K. Mukund, S. Subramaniam, Skeletal muscle: A review of molecular structure and function, in health and disease. *Wiley Interdiscip. Rev. Syst. Biol. Med.* **12**, e1462 (2020).
28. V. Bundhoo, E. Haslam, B. Birch, E. J. Park, A shape memory alloy-based tendon-driven actuation system for biomimetic artificial fingers, part I: Design and evaluation. *Robotica* **27**, 131–146 (2009).
29. Y. Au, The muscle ultrastructure: A structural perspective of the sarcomere. *Cell. Mol. Life Sci.* **61**, 3016–3033 (2004).
30. S. L. Hume, S. M. Hoyt, J. S. Walker, B. V. Sridhar, J. F. Ashley, C. N. Bowman, S. J. Bryant, Alignment of multi-layered muscle cells within three-dimensional hydrogel macrochannels. *Acta Biomater.* **8**, 2193–2202 (2012).
31. C. Ayres, G. L. Bowlin, S. C. Henderson, L. Taylor, J. Shultz, J. Alexander, T. A. Telemeco, D. G. Simpson, Modulation of anisotropy in electrospun tissue-engineering scaffolds: Analysis of fiber alignment by the fast Fourier transform. *Biomaterials* **27**, 5524–5534 (2006).
32. D. E. Rassier, B. R. MacIntosh, W. Herzog, Length dependence of active force production in skeletal muscle. *J. Appl. Physiol.* **86**, 1445–1457 (1999).
33. R. G. Dennis, P. E. Kosnik, Excitability and isometric contractile properties of mammalian skeletal muscle constructs engineered in vitro. *In Vitro Cell. Dev. Biol. Anim.* **36**, 327–335 (2000).
34. Y. Yamamoto, A. Ito, H. Fujita, E. Nagamori, Y. Kawabe, M. Kamihira, Functional evaluation of artificial skeletal muscle tissue constructs fabricated by a magnetic force-based tissue engineering technique. *Tissue Eng. Part A* **17**, 107–114 (2011).
35. D. G. Allen, G. D. Lamb, H. Westerblad, Skeletal muscle fatigue: Cellular mechanisms. *Physiol. Rev.* **88**, 287–332 (2008).
36. Y. Kagawa, H. Miyahara, Y. Ota, S. Tsuneda, System for measuring oxygen consumption rates of mammalian cells in static culture under hypoxic conditions. *Biotechnol. Prog.* **32**, 189–197 (2016).
37. T. L. Place, F. E. Domann, A. J. Case, Limitations of oxygen delivery to cells in culture: An underappreciated problem in basic and translational research. *Free Radic. Biol. Med.* **113**, 311–322 (2017).
38. D. Hu, D. Howard, L. Ren, Biomechanical analysis of the human finger extensor mechanism during isometric pressing. *PLOS ONE* **9**, e94533 (2014).
39. A. W. Racca, A. E. Beck, V. S. Rao, G. V. Flint, S. D. Lundy, D. E. Born, M. J. Bamshad, M. Regnier, Contractility and kinetics of human fetal and human adult skeletal muscle. *J. Physiol.* **591**, 3049–3061 (2013).
40. B. Jo, K. Motoi, Y. Morimoto, S. Takeuchi, Dynamic and static workout of in vitro skeletal muscle tissue through a weight training device. *Adv. Healthc. Mater.* **13**, 2401844 (2024).
41. J. W. Fleming, A. J. Capel, R. P. Rimington, P. Wheeler, A. N. Leonard, N. C. Bishop, O. G. Davies, M. P. Lewis, Bioengineered human skeletal muscle capable of functional regeneration. *BMC Biol.* **18**, 145 (2020).
42. A. Grosberg, A. P. Nesmith, J. A. Goss, M. D. Brigham, M. L. McCain, K. K. Parker, Muscle on a chip: Contractility assays for smooth and striated muscle. *J. Pharmacol. Toxicol. Methods* **65**, 126–135 (2012).
43. L. Madden, M. Juhas, W. E. Kraus, G. A. Truskey, N. Bursac, Bioengineered human myobundles mimic clinical responses of skeletal muscle to drugs. *eLife* **4**, e04885 (2015).
44. M. A. Ortega, X. Fernández-Garibay, A. G. Castaño, F. De Chiara, A. Hernández-Albors, J. Balaguer-Trias, J. Ramón-Azcón, Muscle-on-a-chip with an on-site multiplexed biosensing system for monitoring of secreted IL-6 and TNF-α. *Lab Chip* **19**, 2568–2580 (2019).
45. O. Aydin, X. T. Zhang, S. Nuethong, G. J. Pagan-Diaz, R. Bashir, M. Gazzola, M. T. A. Saif, Neuromuscular actuation of biohybrid motile bots. *Proc. Natl. Acad. Sci. U.S.A.* **116**, 19841–19847 (2019).
46. K. Yamamoto, N. Yamaoka, Y. Imaizumi, T. Nagashima, T. Furutani, T. Ito, Y. Okada, H. Honda, K. Shimizu, Development of a human neuromuscular tissue-on-a-chip model on a 24-well-plate-format compartmentalized microfluidic device. *Lab Chip* **21**, 1897–1907 (2021).
47. R. P. Rimington, J. W. Fleming, A. J. Capel, P. C. Wheeler, M. P. Lewis, Bioengineered model of the human motor unit with physiologically functional neuromuscular junctions. *Sci. Rep.* **11**, 11695 (2021).
48. T. Li, M. Nie, Y. Morimoto, S. Takeuchi, Pillar electrodes embedded in the skeletal muscle tissue for selective stimulation of biohybrid actuators with increased contractile distance. *Biofabrication* **16**, 035022 (2024).

Acknowledgments: We thank K. Nogami, S. Funatani, and Y. Matsumura for support in setting up the experimental environment. **Funding:** This work was supported by the JST-Mirai Program JPMJMI20C1, JST Fusion Oriented Research for Disruptive Science and Technology JPMJFR222Q, JSPS KAKENHI grant number JP21H05013, and UTEC-UTokyo FSI Research Grant Program. **Author contributions:** All authors planned the experiment and contributed to the analysis of the data and discussion. X.R. performed and Y.M. and S.T. supervised the experiment. All authors wrote the paper. **Competing interests:** The authors declare that they have no competing interests. **Data and materials availability:** All data are presented in the paper and/or the Supplementary Materials. The data for this study have been deposited in the Dryad database with DOI 10.5061/dryad.xd2547drh.

Submitted 5 July 2024
Accepted 16 January 2025
Published 12 February 2025
10.1126/scirobotics.adr5512

Science Robotics

Biohybrid hand actuated by multiple human muscle tissues

Xinzhu Ren, Yuya Morimoto, and Shoji Takeuchi

Sci. Robot. **10** (99), eadr5512. DOI: 10.1126/scirobotics.adr5512

Science Robotics (ISSN 2470-9476) is published by the American Association for the Advancement of Science. 1200 New York Avenue NW, Washington, DC 20005. The title *Science Robotics* is a registered trademark of AAAS.